THE EUROPEAN
PHYSICAL JOURNAL B

First principles study of the electronic structures of erbium silicides with non-frozen 4f treatment

C.L. Ma[1,2], S. Picozzi[3], X. Wang[1], and Z.Q. Yang[1,a]

[1] Surface Physics Laboratory (National Key Laboratory), Fudan University, Shanghai 200433, China
[2] Department of Applied Physics, University of Science and Technology of Suzhou, Suzhou 215011, China
[3] CNR-INFM, CASTI Regional Laboratory, 67100 Coppito (L'Aquila), Italy

Abstract. The electronic structures (especially $4f$ states) of hexagonal and tetragonal erbium silicides are investigated within density functional theory. Contrary to previous theoretical studies on these compounds, Er $4f$ electrons are treated as valence state electrons, explicitly taking into account the on-site Coulomb interactions. Total energy calculations show that the relaxed hexagonal $ErSi_{1.7}$ is more stable than the tetragonal structure, consistently with related experimental observations. The calculated total density of states of the hexagonal $ErSi_{1.7}$ agrees well with the experimental valence-band spectrum in a wide energy range from 0 to 12 eV below the Fermi level. In addition, our study indicates that the occupied $4f$ states in erbium silicides can also locate in the energy range of 0–4.0 eV below the Fermi energy, much different from the prediction of the previously adopted Er ion model.

PACS. 71.15.Mb Density functional theory, local density approximation, gradient and other corrections – 71.20.Ps Other inorganic compounds – 71.27.+a Strongly correlated electron systems

1 Introduction

Films of erbium silicides have drawn considerable attention in the past few decades [1–10]. Erbium silicide possesses low resistivity [11] and $ErSi_2$/Si contact on n-type Si presents exceptionally low Schottky barrier heights [9], making this material be useful for ohmic or rectifying contacts, and low-resistance interconnects in large scale integrated circuits [9,6]. Recently, erbium silicide was demonstrated to self-assemble into nano-scale structures, such as quasi-one dimensional nanowires and quasi-zero dimensional nano-islands [12–14], which may find applications in small quantum devices in future.

Up to now, the experimental investigations of erbium silicides were all carried out for the thin films grown on Si substrates. The crystal structure of epitaxially grown erbium silicides depends on the growth condition. For the films grown on Si(111), there appears only the hexagonal AlB_2 phase whose lattice mismatch to Si(111) is only −1.22% [8]. For films grown on Si(100) substrate [4,15,16], both hexagonal AlB_2 and tetragonal $ThSi_2$ phases are observed, although from the viewpoint of lattice mismatch, the tetragonal phase would be the favorable structure, since the mismatch of tetragonal $ErSi_2$/Si(100) is 3.1%, smaller than that of 6.5% for hexagonal $ErSi_2$/Si(100). In addition, experiments have found that the ideal stoichiometry of hexagonal $ErSi_2$ can be obtained only in the case of very thin films with thickness being one mono-

layer [5]. The structure of thicker film is a nonstoichiometric $ErSi_{1.7}$ [8,17], which contains about 20% of silicon vacancies, namely, one Si atom out of six is missing in each hexagonal Si ring. Moreover, the silicon vacancies were found to array orderly in the structure [13,18]. The period of silicon vacancies along [0001] or c_{hex} axis has been suggested to be either $1c$ (where c is the lattice constant along the hexagonal axis) with silicon vacancies stack on top of each other along c_{hex} [18], or $2c$ with the neighboring vacancy-containing silicon layers rotated by 120 degrees with each other [13]. These two cases are labeled as Er_3Si_5 and Er_6Si_{10} in our paper later. The above experimental facts concerning the structural stability of different erbium silicide phases and the silicon vacancy ordering in hexagonal erbium silicides have not been clarified in previous theoretical studies.

Several groups [19–21] have investigated the electronic structures of hexagonal $ErSi_2$ and $ErSi_{1.7}$. Magaud et al. [19] first presented the theoretical study of the electronic structure of stoichiometric $ErSi_2$ using the self-consistent augmented-plane-wave band calculation. The calculated and experimental valence-band results were found to agree only qualitatively in a narrow energy range. Stauffer et al. [20] studied the electronic structures of both $ErSi_2$ and $ErSi_{1.7}$ by the extended Hückel theory, which is believed to be an empirical method so that its results strongly depend on the parameters chosen. Later, Allan et al. [21] have reported the calculations of $ErSi_2$ and $ErSi_{1.7}$ by means of the linear-muffin-tin-orbital method

[a] e-mail: `zyang@fudan.edu.cn`
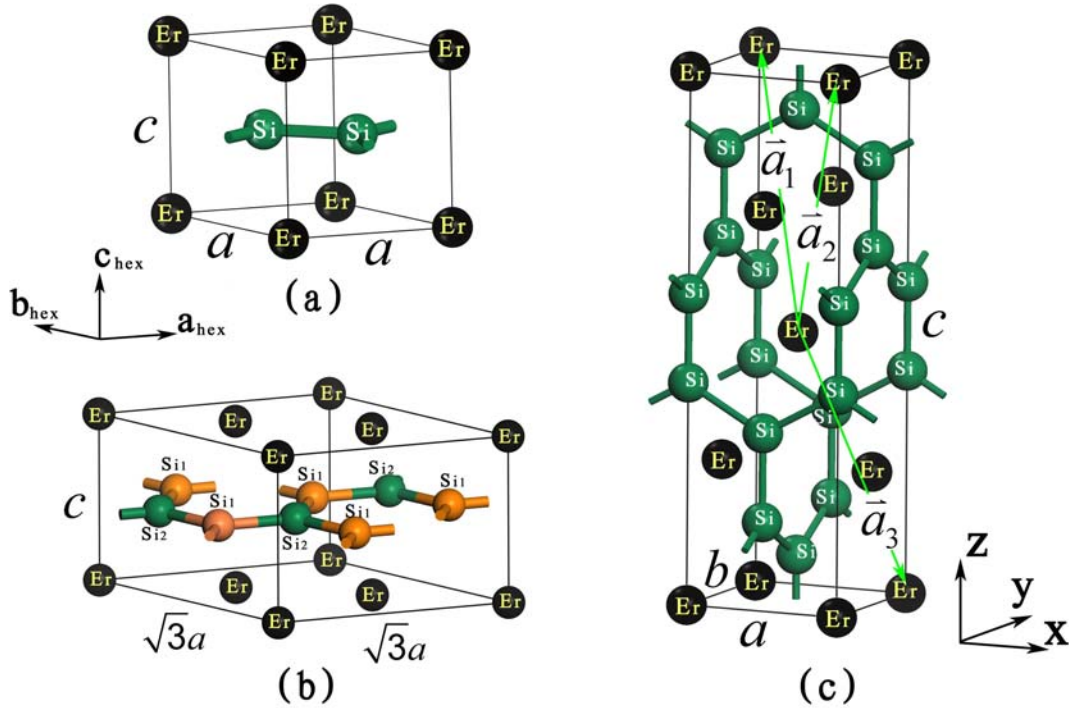
Fig. 1. Unit cells of ideal hexagonal $ErSi_2$ (a), vacancy-containing hexagonal Er_3Si_5 (before relaxation) (b), and crystal cell of tetragonal $ErSi_2$ (c). The vectors $\vec{a}_1$, $\vec{a}_2$ and $\vec{a}_3$ in (c) indicate the primitive translations of tetragonal $ErSi_2$. The coordinates chosen are hexagonal in (a), (b), and Cartesian in (c).

and the tight-binding method. Due to the difficulty in treating the strong correlated $4f$ electrons, the Er $4f$ were forced in the core states ('frozen $4f$') in all the above studies. They could compare the electronic structures with experimental x-ray photoelectron spectroscopy (XPS) measurements [17,22] only in the energy range of 0–4.0 eV below the Fermi level (E_F), since Er $4f$ were believed not to locate in this energy range according to the previous Er ion model [23]. The 'frozen $4f$' approximation, however, was not always believed to be unquestionable when describing Er-Si interactions. Rossi in his photoemission measurements verified that the $4f$ orbitals of rare-earth elements would hybridize with the Si valence band [24]. Later Gan et al. [25], Wan et al. [26] and Fu et al. [27] all treated the Er $4f$ orbitals as valence states to describe the interaction of Er and host Si atoms in calculating the electronic structures of Er-containing materials.

In the present work, we study the electronic structures of erbium silicides by means of the local density functional theory with the inclusion of on-site Coulomb interaction U for the strong correlated $4f$ electrons (LDA+U method) [28,29]. All the $4f$ electrons in the calculations are treated as valence state electrons. The total energy calculations show that the relaxed hexagonal $ErSi_{1.7}$ is more stable than the tetragonal structure, which, together with the mismatch conditions, explains the experimental observation of both AlB_2 and $ThSi_2$ phases for the compound grown on Si (100). The relief of the frozen $4f$ electrons

gives rise to some new features concerning the interactions between the orbitals of constituent atoms. The calculated total density of states (TDOS) of the hexagonal $ErSi_{1.7}$ structure is found to agree well with experimental valence-band spectrum in a wide energy range. The detailed analysis of the partial DOS (PDOS) of Er and Si atoms are presented.

2 Structural models and calculation details

We investigate comparatively the electronic structures of several types of erbium silicides, i.e., the ideal hexagonal $ErSi_2$ ($ErSi_2(H)$), the vacancy-containing hexagonal Er_3Si_5, Er_6Si_{10} and the tetragonal $ErSi_2$ ($ErSi_2(T)$). The unit cells of hexagonal structures studied are shown in Figure 1a and b. The lattice parameters were taken from experimental data, $a = 3.79$ Å and $c = 4.09$ Å [4]. The unit cell of hexagonal Er_6Si_{10} (not shown here) is doubled with respect to hexagonal Er_3Si_5 in c_{hex} direction and the neighboring vacancy-containing silicon layers rotate by 120 degrees relative to each other [13]. Figure 1c gives the crystal cell of tetragonal $ErSi_2$ structure, where the vectors $\vec{a}_1$, $\vec{a}_2$ and $\vec{a}_3$ indicate the primitive translations of tetragonal $ErSi_2$. The lattice parameters used were $a = b = 3.96$ Å and $c = 13.26$ Å [4].

The calculations were performed by means of the linear muffin-tin orbitals method within atomic-sphere

Table 1. Total energies of $ErSi_2(H)$, $ErSi_2(T)$ and vacancy-containing hexagonal Er_3Si_5 before and after relaxation (denoted as Er_3Si_5(unre.) and Er_3Si_5(re.), respectively) calculated by the full-potential LMTO method. All the total energies are referred to that of $ErSi_2(H)$.

Crystal Structure	$ErSi_2(H)$	$ErSi_2(T)$	Er_3Si_5(unre.)	Er_3Si_5(re.)
Total Energy (eV/$ErSi_2$ unit cell)	0	−0.51	0.35	−1.58

approximation (LMTO-ASA) [30] and the more accurate full-potential LMTO (FLMTO) method [31]. For the LMTO-ASA calculation, empty spheres, when needed, were inserted into proper places in the unit cell to guarantee the structures to be closely packed. The states of Er $6s$, $5p$, $5d$, $4f$ and Si $3s$, $3p$, $3d$ were taken as the basis set in the calculation. The states of Er $5s$ were treated as semicore ones. The radii of muffin-tin-spheres of Er and Si were taken as 1.89 and 1.09 Å, respectively. Within the atomic spheres, the basis function, charge density and potential were expanded in spherical harmonics and radial functions. The radial part of the basis was obtained by solving Kohn-Sham equations in which semi-relativistic corrections were incorporated. The local exchange-correlation potential of Vosko-Wilk-Nussair [32] type was employed in the calculation. The integration over the Brillouin zone was performed using the tetrahedron method. The reliability of LMTO-ASA method was judged by comparing its results with those from FLMTO method. The FLMTO method combines features of the LMTO, linearized augmented plane-wave (LAPW) [33] and projector augmented-wave (PAW) [34] approaches. It is well known that the FLMTO gives more accurate total energies than LMTO-ASA; however, the differences between the densities of states obtained by using the two methods are negligible. Therefore, the total energies of all the erbium silicides are calculated within the FLMTO method, whereas the DOSs shown in this paper are obtained with the LMTO-ASA approach.

In order to describe Er $4f$ states correctly, the LDA + U approach proposed by Anisimov et al. [28,29,35] was employed in the calculation. The details of the method can be found in references [28,29,35,36]. For the average Coulomb U parameter of Er $4f$, we consider a series of values ranging from 3.0 and 7.0 eV, and find that the best fit of the calculated total density of states of Er_3Si_5 to the experimental XPS data can be reached at U = 6.2 eV. Thus the optimized value of U is determined to be 6.2 eV, which is very close to the result of Huang et al. [37]. The exchange parameter J was fixed at 0.8 eV.

3 Results and discussion

3.1 Structural stability

In order to compare the stability of different erbium silicide structures, we calculated their total energies. The results are given in Table 1, where the total energy of $ErSi_2(H)$ is chosen as the reference. Since the numbers of atoms in the unit cells of different structures are different, the calculated total energies must be normalized to that of

an $ErSi_2$ cell. The way we employed for non-stoichiometric Er_3Si_5 was to calculate the energy of one bulk Si atom plus the energy of an Er_3Si_5 cell and divide the sum by three. In Er_3Si_5, the Si atoms surrounding the Si vacancy are allowed to relax along all the three directions, while the calculation results show that only the Si atoms in the vacancy-containing layer relax laterally within the Si plane with a displacement of less than 0.38 Å for the first nearest neighbors of the vacancy.

It can be seen from Table 1 that the total energy of $ErSi_2(T)$ is lower than that of $ErSi_2(H)$. The nonstoichiometric structure Er_3Si_5 without relaxation of Si atoms neighboring to the vacancies is not stable compared to the ideal $ErSi_2(H)$ and $ErSi_2(T)$. However, after relaxation, the total energy of Er_3Si_5 becomes the lowest one, consistently with the experimental observation that the hexagonal erbium silicides usually contain Si vacancies.

Although the tetragonal $ErSi_2$ is not the most stable structure in terms of its total energy, it can be grown on Si(100) experimentally. This might be due to the existence of strain energy induced by the lattice mismatch in the experimental film. The lattice mismatch between $ErSi_2$ and Si(100) is 6.5% and 3.1% for hexagonal and tetragonal films, respectively. The relatively smaller lattice mismatch and thus the smaller strain energy for $ErSi_2(T)$/Si (100) can partially compensate the larger bulk energy of this film. Therefore the appearance of $ErSi_2(T)$ on Si (100) can also be expected. Of course, a thorough investigation on the stability of these two phases should take precisely into account the strain energy which depends strongly on the growth condition. This would not be easy to consider and goes beyond the scope of the present paper.

3.2 Electronic density of states

3.2.1 Hexagonal $ErSi_2$ phase

The TDOSs of hexagonal $ErSi_2$ obtained by LDA+U at different values of U (0, 4.0, 5.0, 6.2 eV) are shown in Figure 2a–d. In the case when the on-site Coulomb interactions are not considered (LDA, U = 0), a huge peak of Er $4f$ states is located unreasonably at E_F. It means that without considering the strong correlation effect, the de-freezing of Er $4f$ electrons cannot give correct TDOS for erbium silicide. With the increase of U, the $4f$ states become much broader, and the occupied $4f$ states move to a lower energy region, while the unoccupied ones shift to high energy region gradually. This trend is similar to what happens to $3d$ electrons in transition group atoms when they are treated with the LDA+U method [36]. It is also found that other states in the region of $-12 \sim -7$ eV and
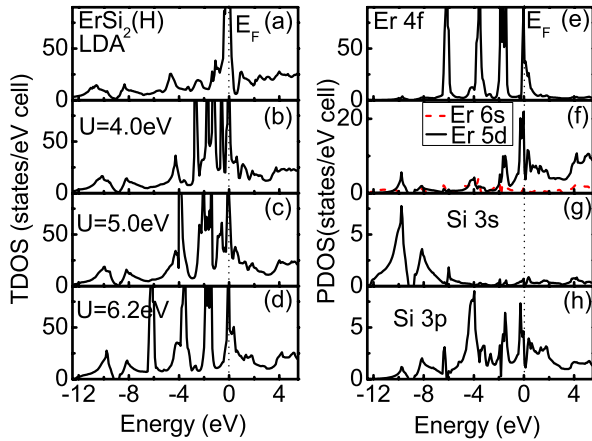
Fig. 2. (a)-(d) TDOSs of ideal hexagonal $ErSi_2$ obtained by using LDA+U at U = 0, 4.0, 5.0 and 6.2 eV, respectively. (e)-(h) PDOSs of hexagonal $ErSi_2$ calculated at U = 6.2 eV.

Fig. 3. (a) Calculated TDOSs of hexagonal Er_3Si_5 (solid curve) and Er_6Si_{10} (dashed curve) (U = 6.2 eV). (b) The experimental XPS (from Paki et al. [17]).

$3 \sim 5$ eV, change with U too, indicating the hybridization between $4f$ and other states. When U = 6.2 eV, there are mainly four peaks in the DOS, located at about -6.0, -4.0, -1.8 eV and around E_F. This result is quite different from those by Magaud et al. [19] and Allan et al. [21]. Although there is lack of experimental data to judge which result would be the correct one, the big differences between the TDOSs of $ErSi_2$ of our results and theirs will give some information on the effect of de-freezing of $4f$ electrons.

The PDOSs of Er and Si states in hexagonal $ErSi_2$ are shown in Figure 2e–h. It can be seen that the states around E_F in Figure 2d are mainly composed of Er $4f$, $5d$ and Si $3p$, which are hybridized significantly. The originally empty Er $5d$ states now become partially occupied due to the charge transfers (partly from Er $6s$ and partly from Er $4f$). This behavior makes Er $5d$ play an important role in the electronic structure of erbium silicides. We can also see that Er $4f$ can affect the distribution of Si $3p$ through Er $5d$, and may therefore change relevant properties, such as the conductivity of the compound. There are about 0.2 e charge transferred from Er to Si $3p$ states. This little charge transfer reveals the covalent effect between Er-Si atoms. Magaud et al. [19] and Allan et al. [21] also presented the PDOSs of ideal hexagonal $ErSi_2$. Their PDOSs of Er $6s$, $5d$ and Si $3s$, $3p$ are very different from ours shown in Figure 2. This difference can be expected, because they treated the Er $4f$ orbitals as 'frozen cores'.

3.2.2 Hexagonal $ErSi_{1.7}$ phase

Our calculations demonstrated that in non-stoichiometric Er_3Si_5 and Er_6Si_{10} the structural relaxation, which can drastically lower the total energy as described above, gives only little effect on the distribution of the electronic states, so its effect was ignored in the following analysis of DOSs. Figure 3a shows the TDOS of Er_3Si_5 (solid line) in the energy ranges of 0–12 eV below E_F. The value of U used
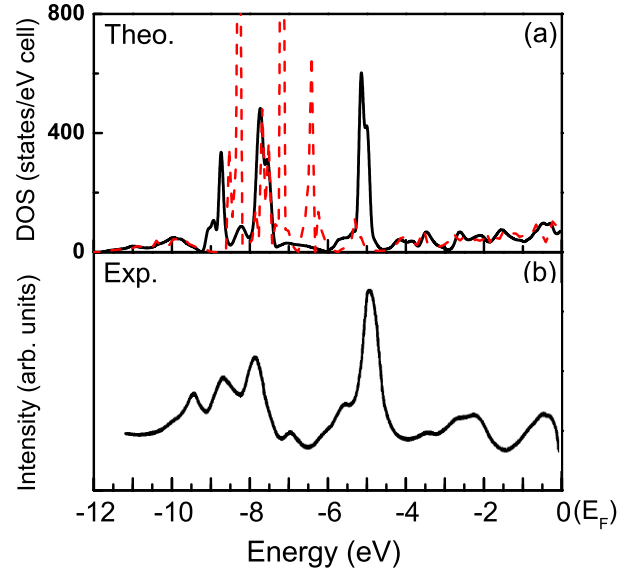
in the LDA + U calculation was optimized to be 6.2 eV, close to the value used for Er $4f$ by Fu et al. [27] and Huang et al. [37]. The typical experimental XPS spectrum [7,17,22] in the same energy range is shown in Figure 3b. It is quite obvious that our theoretical TDOS of Er_3Si_5 agrees with experiment much better than all the previous theoretical calculations [19,21], especially the Er $4f$ multiplet components in the energy range of -4 to -10 eV. Not only the peak shapes and positions coincide fairly well, but also the relative intensities of these peaks are almost the same as that in the experiment. In the energy range of 0 to -4 eV, the main features of the calculated TDOS seems in agreement with the experimental spectrum, but the fine structures in the calculated TDOS is smeared out by a big background signal superposed on the valence states of $ErSi_{1.7}$ in the XPS spectrum.

The TDOS of Er_6Si_{10} is shown as dashed curves in Figure 3a. The result deviates remarkably from the experiment, suggesting that the period of vacancy layers in $ErSi_{1.7}$ along c_{hex} is $1c$ rather than $2c$, in agreement with the result of Knapp et al. [18].

The origin of the peaks in Er_3Si_5 can be clarified more clearly in terms of the PDOS of Er $4f$, $6s$, $5d$ and Si $3s$, $3p$ shown in Figure 4a–d. Besides the $4f$ multiplet components in the energy range of -4 to -10 eV, there are considerable PDOS of Er $4f$ in the energy range of 0 to -4 eV, which is shown by rescaling the y-values in Figure 4a. For the PDOS of Si atoms, we must notice that in Er_3Si_5, there are two types of Si atoms around the vacancy in the unit cell, i.e., the first nearest neighbor Si atoms of the vacancy (labeled as Si_1) and the second neighbor ones (labeled as Si_2) (see Fig. 1b). Their PDOSs differ slightly as shown in Figure 4c and d. The PDOS of Si_1 $3s$ shows a strong peak at about -8.4 eV which is identified to be
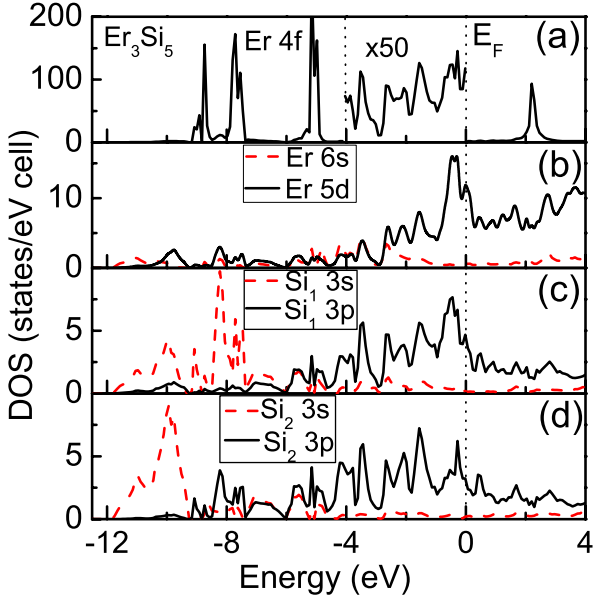
Fig. 4. Calculated PDOSs for hexagonal Er_3Si_5 (U = 6.2 eV). (a) Er $4f$, (b) Er $6s$ (dashed) and $5d$ (solid), (c) Si_1 $3s$ (dashed) and $3p$ (solid), and (d) Si_2 $3s$ (dashed) and $3p$ (solid).

Fig. 5. (a) TDOS of tetragonal $ErSi_2$. (b)–(d) PDOSs of Er $4f$, Er $6s$ (dashed) and $5d$ (solid), Si $3s$, and Si $3p$, respectively. The U value used is 6.2 eV.

related to the Si vacancy because this peak does not exist in the PDOS of vacancy-free $ErSi_2$ shown in Figure 2g. The peak near -10 eV appeared in both the PDOSs of Si_1 $3s$ and Si_2 $3s$ can also be seen in the PDOS of Si $3s$ of $ErSi_2$, so it should represent the bulk property. The Si_1 atom, having a vacancy adjacent to it, can only form two Si-Si covalent bonds with its neighboring Si atoms, so its $3p$ forms stronger bonds with Er $5d$ than Si_2 does (see Fig. 4b, c and d). This strong interaction repulses the Er $4f$ states to move far away from E_F. By comparing the PDOSs of Er_3Si_5 in Figure 4 and TDOS in Figure 3a in the range of 0–4 eV below E_F, one can see that the peak structures in that energy range are mainly caused by the hybridization of different components of Er $4f$, $5d$ and $(Si_1 Si_2)$ $3p$. This in turn illustrates that treating Er $4f$ states as valence states instead of core states is reasonable.

In previous work, the PDOS of $ErSi_{1.7}$ has only been given by Allan et al. [21]. In their PDOSs, Er atom does not contribute much to the states in the valence band, and the experimentally observed $4f$ multiplet components in the energy range of -4 to -10 eV do not appear in their TDOS due to the 'frozen $4f$' model they used. So the overall coincidence of their TDOS and the experiment is not satisfactory.

3.2.3 Tetragonal $ErSi_2$ phase

Figure 5 shows the TDOS and PDOSs of $ErSi_2$(T) calculated by using LDA+U method. In the TDOS, there are two main peaks at the energies of -6 and -8 eV, and some features in the energy range of 0–4 eV below E_F. The TDOS here is quite different from that of $ErSi_2$(H)

shown in Figure 2d, although these two phases possess the same stoichiometric composition. This fact indicates that the electronic states of erbium silicides depend not only on their stoichiometries but also strongly on their crystal structures. Because of the lack of experimental valence band spectrum of $ErSi_2$(T) in the previous literatures, we cannot judge our results by comparing them with experiment, whereas they provide a theoretical prediction of the valence band for tetragonal $ErSi_2$ for the future experimental investigations.

Comparing with the PDOSs, the two main peaks in TDOS are believed to be originated from the Er $4f$ states, and the hybridization between the Er $5d$, $4f$, and Si $3p$ in the energy range of 0 to -4 eV is quite obvious. The distribution of Si $3s$ and $3p$ here is similar to some extent to that of $ErSi_2$(H), which means that in the stoichiometric $ErSi_2$, the bulk states of Si do not depend sensitively on the crystal structures. The much difference between the TDOSs of the two $ErSi_2$ structures are mainly attributed to the different contributions of Er atoms.

3.2.4 Symmetric properties of Er $4f$ states

To identify more clearly the characters of Er $4f$ orbitals, we show in Figure 6 the symmetric properties of degenerate Er $4f$ states of $ErSi_2$ (T) and $ErSi_2$(H). Due to the tetragonal symmetry in $x \sim y$ plane, the $4f$ states of $x(5x^2-3) \sim y(5y^2-3)$ and $x(y^2-z^2) \sim y(x^2-z^2)$ are both degenerate for $ErSi_2$(T). They contribute to the peaks located at -6.0 and -8.0 eV in Figure 6a, respectively. In the z direction, the symmetry is different with respect to the $x \sim y$ plane; our calculation shows, however, that the z-related states $z(5z^2 - 3)$ and $z(x^2 - y^2)$ do not differ
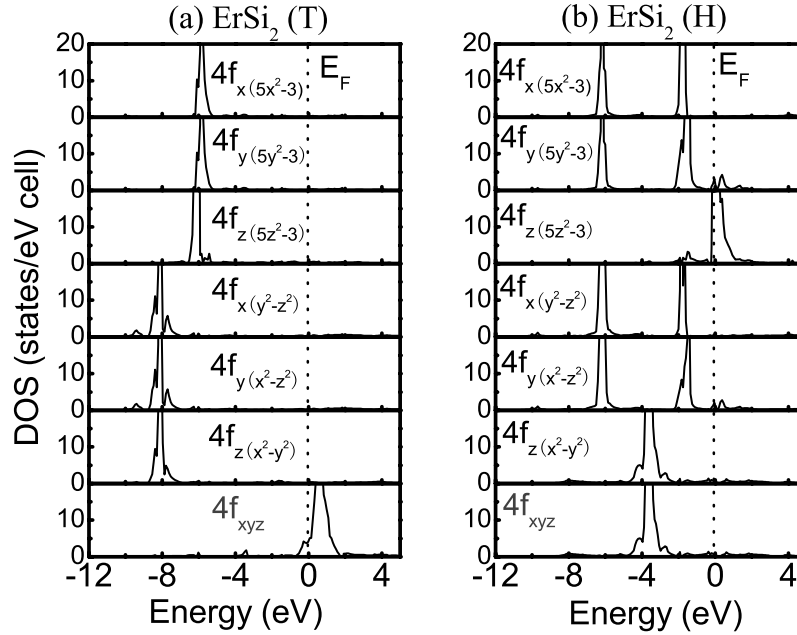
Fig. 6. The symmetric characteristics of Er $4f$ states in (a) ErSi$_2$ (T) and (b) ErSi$_2$(H). The U value used is 6.2 eV.

too much from the corresponding ones in $x \sim y$ plane (see Fig. 6a). This indicates that the lowered symmetry of the compound, with respect to the cubic structure, does not have large effect, which is similar to the behaviors of some slightly distorted compounds such as BaTbO$_3$ [38] etc. Thus, the peaks located at -6.0 and -8.0 eV in Figure 5b are contributed additionally by $z(5z^2 - 3)$ and $z(x^2 - y^2)$ states, respectively. The peak above E$_F$ originates from Er $4f$ xyz state.

The degeneracies of Er $4f$ for ErSi$_2$(H) shown in Figure 6b are very different from that of ErSi$_2$ (T) due to the different crystal symmetries. The single peak of the two-fold degenerate states $x(5x^2 - 3) \sim y(5y^2 - 3)$ in ErSi$_2$(T) splits into two peaks in ErSi$_2$(H), and the distribution of $z(5z^2 - 3)$ state is no longer close to the above two states. The same situation is found for the states $x(y^2 - z^2)$, $y(x^2 - z^2)$ and $z(x^2 - y^2)$. Due to the hexagonal symmetry in ErSi$_2$(H), the states of $z(x^2 - y^2)$ and xyz are found to be degenerate under a $\frac{2\pi}{3}$ rotation along c_{hex}. Now the peaks near -6 and -2 eV are contributed by $x(5x^2 - 3)$, $y(5y^2 - 3)$, $x(y^2 - z^2)$ and $y(x^2 - z^2)$. The $z(x^2 - y^2)$ and the xyz states contribute to the peak near -4 eV, and the $z(5z^2 - 3)$ state contributes to the peak near E$_F$.

3.2.5 Other reasons for the rationality of non-frozen 4f treatment

We have stated above that the calculated total energy and TDOS based on LDA+U method to treat the Er $4f$ as valence states can fit satisfactorily the experimental results. Besides this point, the rationality of our treatment can be further testified by some additional facts.

The Er $4f$ orbitals give significant contribution to the TDOS in the energy range of 0–4 eV below E$_F$ (see Figs. 2, 4, and 5), different from the so called Er ion model [23], which treated the Er $4f$ as core states and found no electronic states in the above energy range for the Er compounds. Previous studies [19–21] actually treated the $4f$ states in erbium silicide by the same way as the Er ion model. However, our calculation on ErSi$_2$ and ErSi$_{1.7}$ does not support this Er ion model.

Under the influence of non-frozen $4f$, the Er $5d$ level in erbium silicides is no longer empty but partially occupied. So, the states located around E$_F$ in TDOS are mainly contributed by Er $4f$, $5d$ and Si $3p$. These states determine the electronic transport properties of the system, giving metallic properties of the materials, in agreement with the electric resistivity measurement done by Travlos et al. [15].

4 Conclusion

We have performed a first principles calculation to investigate the electronic structures of erbium silicides with different structures by treating the Er $4f$ orbitals as valence-states and taking into account the on-site Coulomb interaction of Er $4f$ electrons. The main results are as follows:

(1) The total energy calculations with FLMTO method illustrate that the hexagonal ErSi$_{1.7}$ with the Si atoms adjacent to the vacancies relaxed laterally possesses the lowest relative total energy, thus is the most stable structure on Si(111) and Si(100). When compared with the hexagonal ErSi$_{1.7}$, the tetragonal ErSi$_2$ grown on Si (100) substrate may have a smaller strain energy to compensate its larger bulk energy, thus could be another stable structure observed in the experiment.

(2) An excellent agreement between the theoretical DOS and experimental XPS results is obtained for hexagonal ErSi$_{1.7}$, not only in terms of the energy positions of the main peaks, but also the relative strength of the peaks. From the calculated DOSs, the period of vacancy layers along c$_{hex}$ axis in ErSi$_{1.7}$ is believed to be $1c$ rather than $2c$.

(3) The TDOSs and PDOSs of stoichiometric hexagonal and tetragonal ErSi$_2$ phases have been calculated and compared. The results reveal that the TDOS and PDOS of Er atoms are sensitive to the crystal structure. The calculated TDOS of tetragonal ErSi$_2$ could provide a theoretical prediction of the valence band spectrum for the future XPS experimental study on this rarely investigated structure.

(4) The non-frozen Er $4f$ states are hybridized with other valence states (Er $6s$, $5d$, Si $3s$, $3p$) in all the calculated erbium silicide structures. The contribution of Er $4f$ to the states located within 4 eV below E$_F$ is contrary to the Er ions model applied in previous theoretical studies with frozen core assumption. In conjunction with the above points (1) and (2), all of our results verify the rationality of our non-frozen treatment of Er $4f$ orbitals in erbium silicides.

References

1. E.J. Tan, M.Bouville, D.Z. Chi, K.L. Pey, P.S. Lee, D.J. Srolovitz, C.H. Tung, Appl. Phys. Lett. **88**, 021908 (2006)
2. C. Bonet, I.M. Scott, D.J. Spence, T.J. Wood, T.C.Q. Noakes, P. Bailey, S.P. Tear, Phys. Rev. B **72**, 165407 (2005)
3. C. Rogero, C. Koitzsch, M.E. González, P. Aebi, J. Cerdá, J.A. Martín-Gago, Phys. Rev. B **69**, 045312 (2004)
4. N. Frangis, J. Van Landuyt, G. Kaltsas, A. Travlos, A.G. Nassiopoulos, J. Cryst. Growth **172**, 175 (1997)
5. S. Saintenoy, P. Wetzel, C. Pirri, D. Bolmont, G. Gewinner, Surf. Sci. **331-333**, 546 (1995)
6. L. Pahun, Y. Campidelli, F.A. d'Avitaya, P.A. Badoz, Appl. Phys. Lett. **60**, 1166 (1992)
7. P. Wetzel, L. Haderbache, C. Pirri, J.C. Peruchetti, D.Bolmont, G. Gewinner, Phys. Rev. B **43**, 6620 (1991)
8. J.A. Knapp, S.T. Picraux, Appl. Phys. Lett. **48**, 466 (1986)
9. K.N. Tu, R.D. Thompson, B.Y. Tsaur, Appl. Phys. Lett. **38**, 626 (1981)
10. H. Norde, J. de Sousa Pires, F. d'Heurle, F. Pesavento, S. Petersson, P.A. Tove, Appl. Phys. Lett. **38**, 865 (1981)
11. M. Nishisaka, T. Asano, Jpn. J. Appl. Phys. (Part. I) **37**, 1295 (1998)
12. R. Ragan, Y. Chen, D.A.A. Ohlberg, G.M. Ribeiro, R.S. Williams, J. Cryst. Growth **251**, 657 (2003)
13. W.C. Tsai, H.C. Hsu, H.F. Hsu, L.J. Chen, Appl. Surf. Sci. **244**, 115 (2005)
14. W. Zhou, Y, Zhu, T. Ji, X.Y. Hou, Q. Cai, Nanotech. **17**, 852 (2006)
15. A. Travlos, N. Salamouras, E. Flouda, Appl. Surf. Sci. **120**, 355 (1997)
16. G. Kaltsas, A. Travlos, A.G. Nassiopoulos, N. Frangis, J. Van Landuyt, Appl. Surf. Sci. **102**, 151 (1996)
17. P. Paki, U. Kafader, P. Wetzel, C. Pirri, J.C. Peruchetti, D. Bolmont, G. Gewinner, Phys. Rev. B **45**, 8490 (1992)
18. J.A. Knapp, S.T. Picraux, Mater. Res. Soc. Symp. Proc. **54**, 261 (1986)
19. L. Magaud, J.Y. Veuillen, D. Lollman, T.A.N. Tan, Phys. Rev. B **46**, 1299 (1992)
20. L. Stauffer, C. Pirri, P. Wetzel, A. Mharchi, P. Paki, D. Bolmont, G. Gewinner, Phys. Rev. B **46**, 13201 (1992)
21. G. Allan, I. Lefebvre, N.E. Christensen, Phys. Rev. B **48**, 8572 (1993)
22. P. Wetzel, L. Haderbache, C. Pirri, J.C. Peruchetti, D. Bolmont, G. Gewinner, Surf. Sci. **251-252**, 799 (1991)
23. J.K. Lang, Y. Baer, P.A. Cox, J. Phys. F **11**, 121 (1981)
24. G. Rossi, Surf. Sci. Rep. **1**, 7 (1987)
25. F. Gan, L.V.C. Assali, L.C. Kimerling, Mater. Sci. Forum **96-201**, 579 (1995)
26. J. Wan, L. Ye, Q. Sun, X. Wang, Phys. Rev. B **58**, 10415 (1998)
27. Y. Fu, Z. Huang, X. Wang, L. Ye, J. Phys.: Condens. Matter **15**, 1437 (2003)
28. V.I. Anisimov, J. Zaanen, O.K. Andersen, Phys. Rev. B **44**, 943 (1991)
29. V.I. Anisimov, I.V. Solovyev, M.A. Korotin, M.T. Czyẑyk, G.A. Sawatzky, Phys. Rev. B **48**, 16929 (1993)
30. H.L. Skriver, *The LMTO Method* (Springer, Berlin, 1984)
31. M. Methfessel, M. van Schilfgaarde, *Electronic Structure and Physical Properties of Solids: The uses of the LMTO method*, edited by H. Dreysse (Springer, Heidelberg, 1999), p. 114
32. S.H. Vosko, L. Wilk, M. Nussair, J. Phys. **58**, 1200 (1980)
33. D.J. Singh, *Planewaves, Pseudopotentials, and the APW Method* (Kluwer Academic Publishers, Boston, and references therein, 1994)
34. P.E. Blöchl, Phys. Rev. B **50**, 17953 (1994)
35. V.I. Anisimov, F. Aryasetiawanz, A.I. Lichtenstein, J. Phys.: Condens. Matter **9**, 767 (1997)
36. Z.Q. Yang, Z. Huang, L. Ye, X.D. Xie, Phys. Rev. B **60**, 15674 (1999)
37. Z. Huang, L. Ye, Z.Q. Yang, X. Xie, Phys. Rev. B **61**, 12786 (2000)
38. C.L. Ma, L. Ye, Z.Q. Yang, J. Phys.: Condens. Matter **17**, 7963 (2005)